Theoretical Analysis of Nonlinear Energy Harvesting From Wireless Mobile Nodes

Hiroshi Saito, *Fellow, IEEE*

***Abstract*—This letter provides a theoretical analysis of the radio signal energy harvested from wireless mobile nodes. A nonlinear energy harvesting model based on the research results is proposed. This model is practical but tractable through stochastic geometry. A Gauss-Markov model is used as a mobility model, one that is versatile and can cover various mobile scenarios. The closed form formulas of the first and second moments of the total energy harvested are derived for a combination of these models.**

***Index Terms*—Energy harvesting, nonlinear model, wireless power transfer, Poisson point process (PPP), stochastic geometry, simultaneous wireless information and power transfer (SWIPT).**

I. Introduction

ENERGY harvesting (EH) is promising due to its potential for attaining fully wireless mobile communications [1]. Therefore, a huge number of papers have been published [2]. Such existing studies are based on a linear EH model; that is, the conversion efficiency from the radio frequency (RF) power to the direct current (DC) power is constant and independent of the RF power. However, some studies have shown that the conversion efficiency is not constant and that the harvested DC power becomes saturated as the input RF power increases [3], [4]. Two nonlinear EH models have been proposed on the basis of such studies. One is a sigmoid (logistic) function model [5], [6], [7], [8] and the other is a two-line-segment model [9]. These models revealed that the results on the basis of the conventional linear model can provide serious disagreement with real systems.

In addition to the linear model, the weakness of most existing studies is their focus on fixed nodes as energy sources. Simultaneous wireless information and power transfer (SWIPT) technology has been widely studied, and its progress shows that SWIPT has the potential to make wireless mobile nodes into RF energy sources. Wireless mobile nodes are promising as energy sources due to their rapid growth in number. Unfortunately, however, the performance analysis of EH from wireless mobile nodes is difficult because simulating EH from mobile nodes is time consuming. Thus, theoretical results such as basic statistics on the amount of EH are important. Using such statistics makes it more feasible to evaluate the conditions for certain applications of EH and the performance of EH control algorithms.

Several papers cover EH from/to mobile nodes, but all of them use a linear EH model. One is [10], which covers EH from mobile nodes moving on a straight line with a linear EH model. Another one is [11], where the optimal transmission through the Markov decision process is conducted for mobile nodes harvesting energy. The mobile nodes move from one discrete location to another. The third one is [12], where a single node moves on a straight line between two energy sources to find a better EH location. The reference [8] also investigates a single mobile node. This node is a relay node, and it moves along a predetermined route to offer wireless power transfer to two user nodes. The [13] also considers an optimal EH location from a single dedicated base station and shows that mobility can improve EH performance. The last one [14] assumes the following mobility scenario and analyzes the EH performance through stochastic geometry. When a device has depleted its power after a previous transmission, it checks whether or not its location is within an EH region. If not, the device keeps going straight until it reaches an EH region.

Stochastic geometric analysis for a nonlinear EH model has been conducted, although the wireless nodes are fixed in [15], [16], where the sigmoid nonlinear model was assumed. In [15], the moment generation function for the received RF has been derived. By using it and the gamma distribution approximation, the amount of energy harvested has been evaluated. In [16], a wireless power transfer using millimeter waves has been theoretically analyzed. The amount of energy harvested when the number of antennas becomes infinitely large has been evaluated.

This letter presents an analysis on the energy harvested from mobile nodes where a newly-proposed nonlinear EH model is used. The mobility model used here is a Gauss-Markov model, which is versatile and can cover various mobile scenarios. The nonlinear EH model is simple but well-fitted to measurement data. Most importantly, this model combined with the Gauss-Markov mobility model is tractable in stochastic geometry. Therefore, the closed form formulas of the first and second moment of the total amount of energy harvested can be obtained.

II. Model

A wireless network has a set of nodes $\mathcal{N} \equiv \{X_i\}_{i>0}$. Some nodes appear at t when they are switched on, and their birth locations are modeled by a homogeneous Poisson point process (PPP) $\tilde{\Phi}(t)$ with intensity λ. These nodes are assumed to

Manuscript received April 6, 2021; revised May 20, 2021; accepted June 1, 2021. Date of publication June 3, 2021; date of current version September 9, 2021. This work was supported by KAKENHI JSPS under Grant JP-21K11864. The associate editor coordinating the review of this article and approving it for publication was A. Liu.

The author is with the Mathematics and Informatics Center, University of Tokyo, Tokyo 113-8556, Japan (e-mail: saito@g.ecc.u-tokyo.ac.jp).

Digital Object Identifier 10.1109/LWC.2021.3086192

move. $\mathbf{v}_i(t)$ denotes the movement of X_i at t and is assumed to follow the two-dimension version of the Gauss-Markov mobility model, which has been used in [17], [18], [19].

$$\mathbf{v}_i(t) = \sqrt{1-\zeta^2}\omega(t-1) + \zeta \mathbf{v}_i(t-1) + (1-\zeta)\bar{\mathbf{v}} \quad (1)$$

Here, $\omega(t-1)$ is an independent two-dimension Gaussian random variable with mean 0 and variance matrix V_v, $\bar{\mathbf{v}}$ is an average movement vector, and ζ is a constant. At the birth of X_i, assume that its initial value of $\mathbf{v}_i$ independently follows a known probabilistic distribution function (PDF). Here, assume that this PDF is the normal distribution with mean $\bar{\mathbf{v}}$ and variance matrix V_v. For X_i appearing as a part of $\tilde{\Phi}(t)$, its location $\mathbf{x}_i(s) \in \mathcal{R}^2$ at $s > t$ is given as

$$\mathbf{x}_i(s) = \mathbf{x}_i(t) + \sum_{\tau=t+1}^{s} \mathbf{v}_i(\tau). \quad (2)$$

X_i may disappear at each time slot with probability μ. Let $\Phi(t) \equiv \{\mathbf{x}_i(t)\}_i$ be the set of locations of existing nodes at t. Note that this is also a PPP. Define $\Phi[0, T] \equiv \cup_{s=0}^{T}\Phi(t)$. (For simplicity, [0, T] may be omitted in $\Phi[0, T]$ in the remainder of this letter.)

Let X_0 be a node harvesting energy from other nodes and continuously staying at the origin. Energy is harvested and stored in X_0. Assume that the harvested RF power from X_i is $g\tilde{d}^{-\alpha}$, where $\tilde{d}_i(t) = d_i(t) + \epsilon$ and $d_i(t) \equiv \|\mathbf{x}_i(t)\|$ is the distance between X_0 and X_i at t, $\alpha > 2$ is a path loss exponent, g is the transmission power including gain at t, and ϵ is a small positive constant. Also assume that X_0's DC power converted from the RF power harvested from other nodes at time slot t is given by the following model taking account of non-linear RF-to-DC conversion where $y(t)$ is the output DC power, and ξ is an RF-to-DC conversion function.

$$y(t) = \xi\Big(\sum_{\mathbf{x}_i(t)\in\Phi(t)} g\tilde{d}_i(t)^{-\alpha}\Big) \quad (3)$$

$$\xi(z) = \gamma_{sat} - \gamma_0 \exp(-\beta z) \quad (4)$$

Here, γ_{sat} is a parameter denoting the harvested DC when the received RF power becomes infinitely large, and $\gamma_0, \beta > 0$ are constant parameters. Figure 1 demonstrates the validity of this proposed model. The total energy harvested during [0, T] is $y[0, T] = \sum_{t=0}^{T} y(t)$.

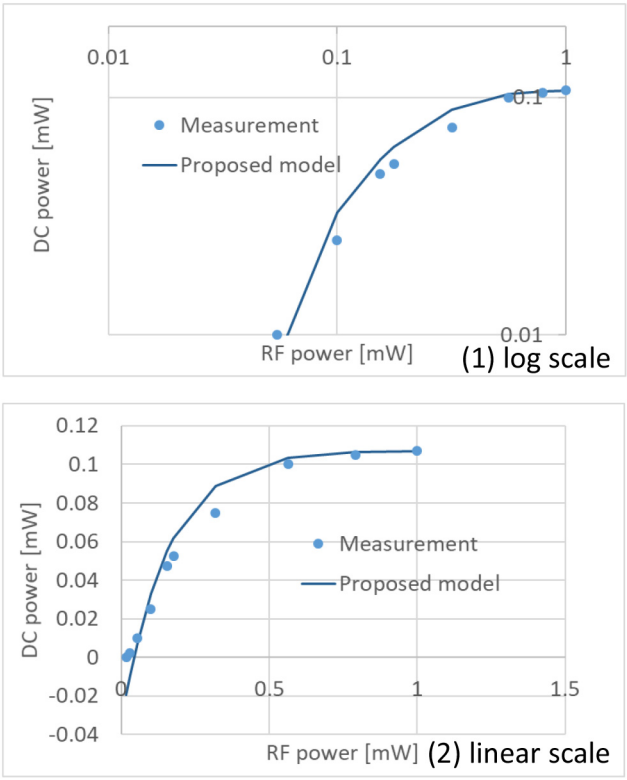

Fig. 1. Received RF power z vs. harvested DC power: proposed model ξ and measurement data regenerated from [6, Fig. 8] for a practical harvesting circuit. γ_{sat}, γ_0, and β used here are 0.1071, 0.14096, and 6.4087.

III. Analysis

This section presents an analysis of the amount of the energy harvested by X_0 from other nodes during [0, T], and a derivation of its first and second moments ($E[y[0, T]]$ and $E[y[0, T]^2]$). For simplicity, $i \in \Phi(t)$ denotes $\mathbf{x}_i(t) \in \Phi(t)$ in the remainder.

A. First Moment of Harvested Energy

Due to Eqs. (3) and (4),

$$E[y(t)] = \gamma_{sat} - \gamma_0 E_{\Phi(t)}\Big[\prod_{i\in\Phi(t)} \exp(-\beta g\tilde{d}_i(t)^{-\alpha})\Big]. \quad (5)$$

Because $\Phi(t)$ is a PPP with intensity $\rho \equiv \lambda/\mu$, use the moment generating functional (MGF) for a PPP (see Remark below). Then, we can obtain

$$E[y[0, T]] = \sum_{t=0}^{T} E[y(t)] = (T+1)(\gamma_{sat} - \gamma_0 A_1(\rho)), \quad (6)$$

where $A_k(\rho) \equiv \exp\{-2\pi\rho\int_0^\infty r(1 - \exp(-k\beta g(\epsilon + r)^{-\alpha}))dr\}$. These equations show that $E[y[0, T]]$ is independent of $\bar{\mathbf{v}}$, V_v, ζ. This is because $\Phi(t)$ is a PPP for any t. (This result is suggested by the displacement theorem for a PPP.) In addition, $E[y[0, T]]$ is independent of λ, μ when ρ is fixed.

Remark: The MGF for a homogeneous PPP $\{\mathbf{x}_i\}_i$ of intensity ρ in Ω is given as follows [20]. For a generic function $h(\mathbf{x})$,

$$E[\prod_i h(\mathbf{x}_i)] = \exp(-\rho\int_\Omega (1 - h(\mathbf{x}))d\mathbf{x}). \quad (7)$$

B. Second Moment of Harvested Energy

As a preliminary, analyze $\Pr(\sum_{\tau=t+1}^{s} \mathbf{v}_i(\tau))$. By using that analysis result, the second moment of harvested energy can be analyzed.

1) Analysis of $\Pr(\sum_{\tau=t+1}^{s} \mathbf{v}_i(\tau))$*:* Because $\mathbf{v}_i(t_0)$ follows $\mathcal{N}(\bar{\mathbf{v}}, V_v)$ at its birth epoch t_0, $\Pr(\mathbf{v}_i(t_0+1)) = \mathcal{N}(\bar{\mathbf{v}}, V_v)$ because of Eq. (1). Thus, for any $t \geq t_0$, $\Pr(\mathbf{v}_i(t)) = \mathcal{N}(\bar{\mathbf{v}}, V_v)$.

By repeatedly applying Eq. (1), for any $\tau \geq t$,

$$\mathbf{v}_i(\tau) = \sqrt{1-\zeta^2}\sum_{k=t}^{\tau-1}\zeta^{\tau-1-k}\omega_i(k) + (1-\zeta^{\tau-t})\bar{\mathbf{v}} + \zeta^{\tau-t}\mathbf{v}_i(t). \quad (8)$$

By using Eq. (8) with $\tau = t+1, \ldots, s$, for $0 \leq \zeta < 1$,

$$\sum_{\tau=t+1}^{s}\mathbf{v}_i(\tau) = \sqrt{1-\zeta^2}\sum_{k=t}^{s-1}\frac{1-\zeta^{s-k}}{1-\zeta}\omega_i(k) + (s-t-\frac{\zeta(1-\zeta^{s-t})}{1-\zeta})\bar{\mathbf{v}} + \frac{\zeta(1-\zeta^{s-t})}{1-\zeta}\mathbf{v}_i(t). \quad (9)$$

By using Eq. (8) for $\zeta = 1$,

$$\sum_{\tau=t+1}^{s}\mathbf{v}_i(\tau) = (s-t)\mathbf{v}_i(t). \quad (10)$$

Because $\Pr(\mathbf{v}_i(t)) = \mathcal{N}(\bar{\mathbf{v}}, V_v)$, $\Pr(\sum_{\tau=t+1}^{s}\mathbf{v}_i(\tau))$ follows $\mathcal{N}((s-t)\bar{\mathbf{v}}, \phi_i(s-t)\,V_v)$, where $\phi_i(s-t) \equiv \frac{1}{(1-\zeta)^2}\{(1-\zeta^2)(s-t) - 2\zeta(1-\zeta^{s-t})\}$ for $0 \leq \zeta < 1$ and $(s-t)^2$ for $\zeta = 1$.

2) Analysis of Second Moment: Note $E[y[0,T]^2] = \sum_{t=0,\ldots,T}E[y(t)^2] + 2\sum_{s>t}E[y(s)y(t)]$. By using the MGF for a PPP,

$$\begin{aligned}E[y(t)^2] &= \gamma_{sat}^2 - 2\gamma_0\gamma_{sat}E_{\Phi(t)}[\prod_{i\in\Phi(t)}\exp(-\beta g\tilde{d}_i(t)^{-\alpha})] \\ &\quad + \gamma_0^2 E_{\Phi(t)}[\prod_{i\in\Phi(t)}\exp(-2\beta g\tilde{d}_i(t)^{-\alpha})] \\ &= \gamma_{sat}^2 - 2\gamma_0\gamma_{sat}A_1(\rho) + \gamma_0^2 A_2(\rho). \end{aligned} \quad (11)$$

For $s > t$,

$$\begin{aligned}&E[y(s)y(t)] \\ &= \gamma_{sat}^2 - 2\gamma_0\gamma_{sat}A_1(\rho) + \gamma_0^2 E_{\Phi(t),\Phi(s)}[\prod_{i\in\Phi(t),j\in\Phi(s)} \\ &\quad \exp(-\beta g(\tilde{d}_i(t)^{-\alpha} + \tilde{d}_j(s)^{-\alpha}))]. \end{aligned} \quad (12)$$

Because $d_i(t)$ and $d_j(s)$ ($i \neq j$) are independently distributed,

$$\begin{aligned}&E_{\Phi(t),\Phi(s)}[\prod_{i\in\Phi(t),j\in\Phi(s)}\exp(-\beta g(\tilde{d}_i(t)^{-\alpha} + \tilde{d}_j(s)^{-\alpha}))] \\ &= E_{\Phi(t)\cap\Phi(s)}[\prod_{i\in\Phi(t)\cap\Phi(s)}\exp(-\beta g(\tilde{d}_i(t)^{-\alpha} + \tilde{d}_i(s)^{-\alpha}))] \\ &E_{\Phi(t)/\Phi(s)}[\prod_{i\in\Phi(t)}\exp(-\beta g\tilde{d}_i(t)^{-\alpha})] \\ &E_{\Phi(s)/\Phi(t)}[\prod_{j\in\Phi(s)}\exp(-\beta g\tilde{d}_j(s)^{-\alpha})]. \end{aligned} \quad (13)$$

Because $\Phi(t)/\Phi(s)$ and $\Phi(s)/\Phi(t)$ are also PPPs with intensity $\rho(1-(1-\mu)^{s-t})$, both of the last two terms of Eq. (13) are $A_1(\rho(1-(1-\mu)^{s-t}))$.

Because the set of node locations $\Phi(t)\cap\Phi(s)$ is also a PPP and because its intensity is $\rho(1-\mu)^{s-t}$,

$$\begin{aligned}&E_{\Phi(t)\cap\Phi(s)}[\prod_{i\in\Phi(t)\cap\Phi(s)}\exp(-\beta g(\tilde{d}_i(t)^{-\alpha} + \tilde{d}_i(s)^{-\alpha}))] \\ &= E_{\Phi(t),\sum_{\tau=t+1}^{s}\mathbf{v}_i(\tau),\mathbf{v}_i(t)}[\prod_{i\in\Phi(t)\cap\Phi(s)} \\ &\quad [\exp(-\beta g((\epsilon + |\mathbf{x}_i(t)|)^{-\alpha} \\ &\quad + (\epsilon + |\mathbf{x}_i(t) + \sum_{\tau=t+1}^{s}\mathbf{v}_i(\tau)|)^{-\alpha}))] \\ &= \int\Psi((s-t)\bar{\mathbf{v}}, \phi_i(s-t)\,V_v)\tilde{B}_{s-t}(\mathbf{u})d\mathbf{u} \\ &\equiv B_{s-t}. \end{aligned} \quad (14)$$

Here, $\Psi((s-t)\bar{\mathbf{v}}, \phi_i(s-t)\,V_v)$ is the PDF of $\mathcal{N}((s-t)\bar{\mathbf{v}}, \phi_i(s-t)\,V_v)$, and

$$\begin{aligned}\tilde{B}_{s-t}(\mathbf{u}) \equiv \exp\{-\rho(1-\mu)^{s-t}\int_0^{\infty}\int_0^{2\pi} \\ r(1-\exp(-\beta g((\epsilon+r)^{-\alpha} \\ + (\epsilon + |(r\cos\psi, r\sin\psi) + \mathbf{u}|)^{-\alpha})))dr\,d\psi\}. \end{aligned} \quad (15)$$

Thus,

$$\begin{aligned}&E[y[0,T]^2] \\ &= (T+1)(\gamma_{sat}^2 - 2\gamma_0\gamma_{sat}A_1(\rho) + \gamma_0^2 A_2(\rho)) \\ &\quad + T(T+1)(\gamma_{sat}^2 - 2\gamma_0\gamma_{sat}A_1(\rho)) \\ &\quad + 2\gamma_0^2\sum_{s>t}B_{s-t}A_1(\rho(1-(1-\mu)^{s-t}))^2. \end{aligned} \quad (16)$$

Because B_{s-t} depends on $s-t$ but not on s or t, the variance $\sigma(y[0,T])^2 \equiv E[y[0,T]^2] - E[y[0,T]]^2$ of $y[0,T]$ is given as follows.

$$\begin{aligned}\sigma(y[0,T])^2 = \gamma_0^2(-(T+1)^2A_1(\rho)^2 + (T+1)A_2(\rho) \\ +2\sum_{k=1}^{T}(T-k+1)B_kA_1(\rho(1-(1-\mu)^k))^2) \end{aligned} \quad (17)$$

When $B_{s-t}A_1(\rho(1-(1-\mu)^{s-t}))^2 = A_1(\rho)^2$ for all $s-t$, $\sigma(y[0,T])^2 = \gamma_0^2(T+1)(A_2(\rho)-A_1(\rho)^2) = \sum_{t=0}^{T}\sigma(y(t))^2$. That is, $\triangle\sigma(y[0,T])^2 \equiv \sigma(y[0,T])^2 - \sum_{t=0}^{T}\sigma(y(t))^2 = 2\gamma_0^2\sum_{k=1}^{T}(T-k+1)(B_{s-t}A_1(\rho(1-(1-\mu)^{s-t}))^2 - A_1(\rho)^2)$ is the effect of the correlations of mobile node locations at different times.

C. Approximation of B_{s-t}

Although Eq. (17) provides $\sigma(y[0,T])^2$, it contains a time-consuming computation for Eq. (14). According to an intensive simulation, $\sigma(y[0,T])$ is almost insensitive to V_v. Thus, B_{s-t} is approximately equal to that with $V_v = 0$, and the computation of B_{s-t} with $V_v = 0$ becomes much easier than that with $V_v \neq 0$. This means that the straight-line mobility model can approximately be used to derive B_{s-t}. An intuitive explanation is as follows. B_{s-t} is determined by the distance from the origin to the location of X_i at t and that at s. X_i may become closer to the origin during $[s, t]$, and X_j may become further away. As a whole, B_{s-t} is almost insensitive to the direction of the movement because $\{X_i\}_i$ is a PPP. The validity of this approximation is demonstrated using numerical examples (see the Appendix).

Because B_{s-t} with $V_v = 0$ is $\tilde{B}_{s-t}((s-t)\bar{\mathbf{v}})$,

$$\begin{aligned}\sigma(y[0,T])^2 \approx \gamma_0^2(-(T+1)^2A_1(\rho)^2 + (T+1)A_2(\rho) \\ +2\sum_{k=1}^{T}(T-k+1)\tilde{B}_k(k\bar{\mathbf{v}})A_1(\rho(1-(1-\mu)^k))^2.) \end{aligned} \quad (18)$$

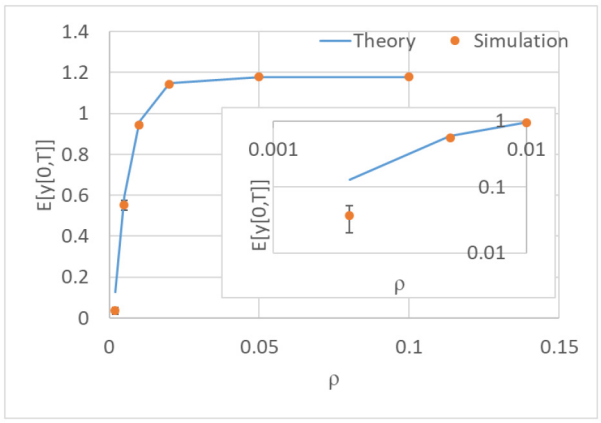

Fig. 2. $E[y[0, T]]$ vs. ρ.

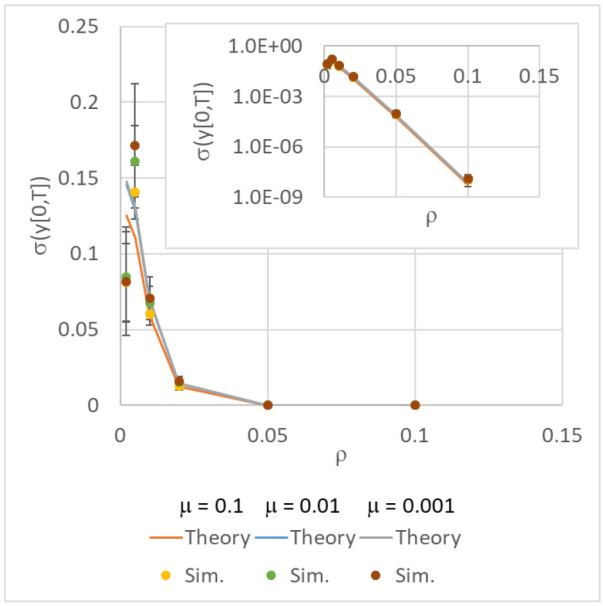

Fig. 3. $\sigma(y[0, T])$ vs. ρ.

IV. Numerical Examples

A. Default Conditions of Numerical Examples

If not explicitly mentioned otherwise, the following conditions were used: $\lambda = 10^{-4}$ (1/m)^2, $\mu = 0.01$, $g = 0.1$ W, $\zeta = 0.9$, $\bar{\mathbf{v}} = (0.5, 0.5)$ m/s (walking speed), $V_v = diag(0.1, 0.1)$ (m/s)^2, $T = 10$, and the time slot length is 1 s. In addition, values of $\gamma_{sat}, \gamma_0, \beta$ in Fig. 1 were used. $\sigma(y[0, T])$, which was calculated theoretically in this section, used the approximation Eq. (18).

Remark: To harvest energy, a minimum power requirement must be satisfied [2]. Here, assume that no EH was obtained in the simulation if the total RF power at each time was less than 0.1 (mW).

B. E[y[0, T]] and $\sigma(y[0, T])$ vs. ρ

Figure 2 plots $E[y[0, T]]$ against ρ, where the simulation results assuming Eq. (4) were with 95% confidential intervals. It clearly demonstrates that $E[y[0, T]]$ becomes saturated as ρ increases, particularly when $\rho > 0.02$. The theoretical results and simulation results were in good agreement. However, for a very small ρ, Eq. (6) overestimated the simulation results. This may have been because Eq. (6) does not take account of the minimum power requirement.

Figure 3 plots $\sigma(y[0, T])$ against ρ. $\sigma(y[0, T])$ showed a sharp decrease as ρ increased. This was because $y[0, T]$ becomes almost constant due to saturation as ρ increases. $\sigma(y[0, T])$ increased as μ decreased (that is, the mean lifetime increased). This was because the number of mobile nodes in $\Phi(t) \cap \Phi(s)$ increases as their lifetimes increase. Thus, the correlations of $y(t)$ and $y(s)$ increase. However, $\sigma(y[0, T])$ is not so sensitive to μ. The theoretical results and simulation results were in good agreement except for a very small ρ.

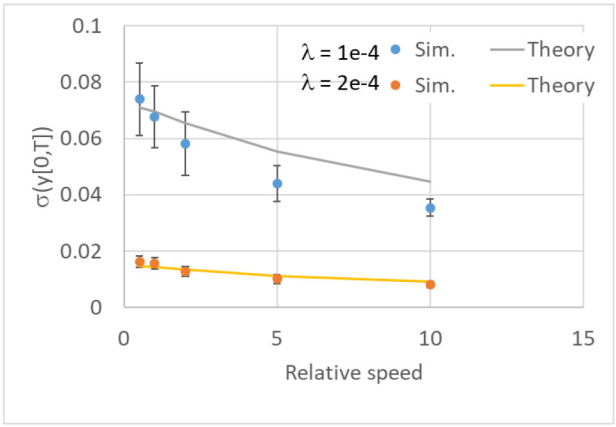

Fig. 4. $\sigma(y[0, T])$ vs. relative speed.

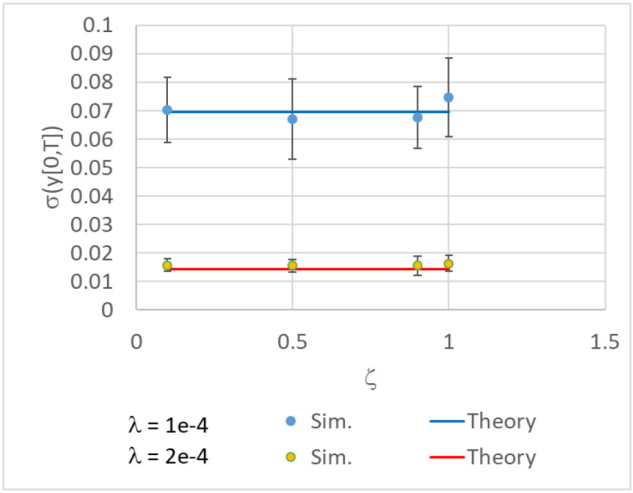

Fig. 5. $\sigma(y[0, T])$ vs. ζ.

C. Effect of Mobility on $\sigma(y[0, T])$

Equation (6) shows that mobility has no effect on $E[y[0, T]]$. However, mobility affects $\sigma(y[0, T])$. This subsection presents a quantitative evaluation of its effect.

Figures 4 and 5 demonstrate the results. The x-axis of Fig. 4 denotes c, where $\bar{\mathbf{v}} = c(0.5, 0.5)$. That is, c is the relative speed against the default $\bar{\mathbf{v}}$. This figure shows that $\sigma(y[0, T])$ decreased as $\bar{\mathbf{v}}$ increased. This is because $\mathbf{x}_i(s)$ was less affected by $\mathbf{x}_i(t)$ as $\bar{\mathbf{v}}$ increased. The theoretical results overestimated the simulation when the relative speed was large with $\lambda = 10^{-4}$.

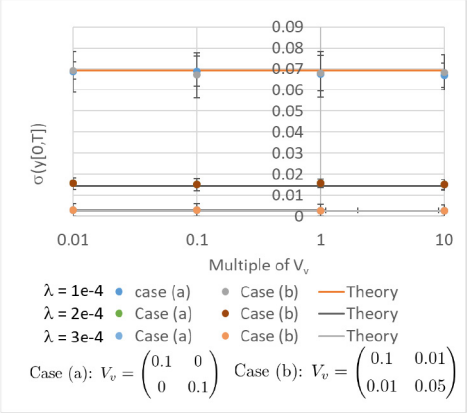

Fig. 6. Comparison of simulation and theory: $\sigma(y[0,\,T])$ vs V_v.

Figure 5 shows that $\sigma(y[0,\,T])$ is almost insensitive to ζ. This is similar to the fact that $\sigma(y[0,\,T])$ is almost insensitive to V_v.

V. Conclusion

This letter provided the closed form formulas for the average and standard deviation of the energy harvested from mobile nodes, where the nonlinear effect of RF-to-DC conversion is taken into account. The mobility model used is a Gauss-Markov model, which is versatile, and stochastic geometry was used as a theoretical tool. The obtained results can contribute to evaluating the conditions for certain applications of EH and the performance of EH control algorithms.

The current model (ξ defined by Eq. (4)) can be extended to cover a wider range of the RF power by introducing multiple exponential functions.

$$\xi(z) = \gamma_{sat} - \sum_k \gamma_k \exp(-\beta_k z) \tag{19}$$

This extension could resolve the problem that the current model provides a negative value of the DC power for a small RF power. The extension of the analysis results in Section III is straightforward for the extended model.

Appendix

This Appendix compares the intensive simulation results regarding $\sigma(y[0,\,T])$ and theoretical $\sigma(y[0,\,T])$ on the basis of the approximation (Eq. (18)) for various V_v. (V_v is $c\begin{pmatrix}0.1 & 0\\ 0 & 0.1\end{pmatrix}$ or $c\begin{pmatrix}0.1 & 0.01\\ 0.01 & 0.05\end{pmatrix}$, where c is an x-axis in Fig. 6.) As Fig. 6 demonstrates, $\sigma(y[0,\,T])$ is almost insensitive to V_v. Thus, the approximation Eq. (18) works.

References

[1] H. Tabassum, E. Hossain, A. Ogundipe, and D. I. Kim, "Wireless-powered cellular networks: Key challenges and solution techniques," *IEEE Commun. Mag.*, vol. 53, no. 6, pp. 63–71, Jun. 2015.

[2] X. Lu, P. Wang, D. Niyato, D. I. Kim, and Z. Han, "Wireless networks with RF energy harvesting: A contemporary survey," *IEEE Commun. Surveys Tuts.*, vol. 17, no. 2, pp. 757–789, 2nd Quart., 2015.

[3] T. Le, K. Mayaram, and T. Fiez, "Efficient far-field radio frequency energy harvesting for passively powered sensor networks," *IEEE J. Solid-State Circuits*, vol. 43, no. 5, pp. 1287–1302, May 2008.

[4] B. Clerckx, "Wireless information and power transfer: Nonlinearity, waveform design, and rate-energy tradeoff," *IEEE Trans. Signal Process.*, vol. 66, no. 4, pp. 847–862, Feb. 2018.

[5] E. Boshkovska, D. W. K. Ng, N. Zlatanov, and R. Schober, "Practical non-linear energy harvesting model and resource allocation for SWIPT systems," *IEEE Commun. Lett.*, vol. 19, no. 12, pp. 2082–2085, Dec. 2015.

[6] B. Clerckx, R. Zhang, R. Schober, D. W. K. Ng, D. I. Kim, and H. V. Poor, "Fundamentals of wireless information and power transfer: From RF energy harvester models to signal and system designs," *IEEE J. Sel. Areas Commu.*, vol. 37, no. 1, pp. 4–33, Jan. 2019.

[7] G. Ma, J. Xu, Y. Zeng, and M. R. V. Moghadam, "A generic receiver architecture for MIMO wireless power transfer with nonlinear energy harvesting," *IEEE Signal Process. Lett.*, vol. 26, no. 2, pp. 312–316, Feb. 2019.

[8] S. Wang, M. Xia, K. Huang, and Y.-C. Wu, "Wirelessly powered two-way communication with nonlinear energy harvesting model: Rate regions under fixed and mobile relay," *IEEE Trans. Wireless Commun.*, vol. 16, no. 12, pp. 8190–8204, Dec. 2017.

[9] J.-M. Kang, I.-M. Kim, and D. I. Kim, "Joint Tx power allocation and Rx power splitting for SWIPT system with multiple nonlinear energy harvesting circuits," *IEEE Wireless Commun. Lett.*, vol. 8, no. 1, pp. 53–56, Feb. 2019.

[10] H. Saito, "Analysis of harvested energy from mobile and fixed nodes," *IEEE Commun. Lett.*, vol. 25, no. 3, pp. 1005–1009, Mar. 2021.

[11] D. Niyato and P. Wang, "Delay-limited communications of mobile node with wireless energy harvesting: Performance analysis and optimization," *IEEE Trans. Veh. Technol.*, vol. 63, no. 4, pp. 1870–1885, May 2014.

[12] A. Arafa and S. Uluku, "Mobile energy harvesting nodes: Offline and online optimal policies," *IEEE Trans. Green Commun. Netw.*, vol. 2, no. 1, pp. 143–153, Mar. 2018.

[13] D. B. Licea, S. A. R. Zaidi, D. McLernon, and M. Ghogho, "Improving radio energy harvesting in robots using mobility diversity," *IEEE Trans. Signal Process.*, vol. 64, no. 8, pp. 2065–2077, Apr. 2016.

[14] S. Kusaladharma, C. Tellambura, and Z. Zhang, "Evaluation of RF energy harvesting by mobile D2D nodes within a stochastic field of base stations," *IEEE Trans. Green Commun. Netw.*, vol. 4, no. 4, pp. 1120–1129, Dec. 2020.

[15] S. Kusaladharma, W.-P. Zhu, W. Ajib, and G. A. A. Baduge, "Stochastic geometry based performance characterization of SWIPT in cell-free massive MIMO," *IEEE Trans. Veh. Technol.*, vol. 69, no. 11, pp. 13357–13370, Nov. 2020.

[16] T. X. Tran, W. Wang, S. Luo, and K. C. Teh, "Nonlinear energy harvesting for millimeter wave networks with large-scale antennas," *IEEE Trans. Veh. Technol.*, vol. 67, no. 10, pp. 9488–9498, Oct. 2018.

[17] B. Liang and Z. J. Haas, "Predictive distance-based mobility management for PCS networks," in *Proc. IEEE INFOCOM*, 1999, pp. 1377–1384.

[18] H. Xiao, X. Zhang, A. T. Chronopoulos, Z. Zhang, H. Liu, and S. Ouyang, "Resource management for multi-user-centric V2X communication in dynamic virtual-cell-based ultra-dense networks," *IEEE Trans. Commun.*, vol. 68, no. 10, pp. 6346–6358, Oct. 2020.

[19] W.-Y. Lee and I. F. Akyildiz, "Spectrum-aware mobility management in cognitive radio cellular networks," *IEEE Trans. Mobile Comput.*, vol. 11, no. 4, pp. 529–542, Apr. 2012.

[20] B. Blaszczyszyn, M. Haenggi, P. Keeler, and S. Mukherjee, *Stochastic Geometry Analysis of Cellular Networks*. Cambridge, U.K.: Cambridge Univ. Press, 2018.